

## Article

# On the Impact of Wavelength Dependency on Supercontinuum Generation in Photonic Crystal Fibers

Antonio Díaz-Soriano <sup>†</sup>, Antonio Ortiz-Mora <sup>†</sup>, David Martínez-Muñoz and Pedro Rodríguez <sup>\*,†</sup>

Physics Department, University of Córdoba, 14014 Andalucía, Spain; f62disoa@uco.es (A.D.-S.); fa2ormoa@uco.es (A.O.-M.); f12mamud@uco.es (D.M.-M.)

\* Correspondence: pm1rogap@uco.es

<sup>†</sup> These authors contributed equally to this work.

**Abstract:** It is common practice when simulating propagation through an optical fiber to assume that its characteristic parameters are constant and determined solely by the central wavelength of the input pulse. In this paper, we propose a study of the impact that the actual wavelength dependence of these parameters has on the propagation results. To this end, simulations were carried out considering both the constant model and the wavelength-dependent model, applying them to the case of the especially sensitive effect of supercontinuum generation in a photonic crystal fiber. The results showed differences of up to 20% of the spectrum and, hence, the importance of taking into account the wavelength dependence of the dispersion fiber parameters to obtain more-realistic results in the simulations.

**Keywords:** numerical simulation; supercontinuum generation; photonic crystal fiber; pulse propagation



**Citation:** Díaz-Soriano, A.; Ortiz-Mora, A.; Martínez-Muñoz, D.; Rodríguez, P. On the impact of wavelength dependency on supercontinuum generation in photonic crystal fibers. *Appl. Sci.* **2024**, *14*, 1429. <https://doi.org/10.3390/app14041429>

Academic Editors: Michael (Misha) Sumetsky, Tomasz Osuch, Davide Careglio and Mirosław Klinkowski

Received: 16 December 2023

Revised: 2 February 2024

Accepted: 6 February 2024

Published: 9 February 2024



**Copyright:** © 2024 by the authors. Licensee MDPI, Basel, Switzerland. This article is an open access article distributed under the terms and conditions of the Creative Commons Attribution (CC BY) license (<https://creativecommons.org/licenses/by/4.0/>).

## 1. Introduction

In applied optics, the introduction of photonic crystals [1] marked an important milestone in the technological ability to control and manipulate light. The photonic crystal functionality is based on its micrometer or nanometer periodic structure scale, so that electromagnetic waves in the visible range will be affected by effects analogous to those suffered by an electron at a periodic potential. This creates a pattern through which photons cannot propagate in certain directions, with different polarization or for certain wavelengths. This is due to the formation of what are known as photonic band gaps. Their application is quite widespread; it has even recently been shown that they can be used for polarization control in metamaterials [2].

The idea of bringing these microstructures to the fiber optic waveguides field led to the introduction of the photonic crystal fibers (PCFs) [3,4], which paved the way to a fresh bunch of new research fields for the photonics community. We can study their use as sensors [5], in high-power generation [6], or as fiber lasers [7], to cite some. Among these new applications, supercontinuum generation by means of a PCF emerged as an easy way to cause a significant broadening in the spectral bandwidth of an input pulse propagating through the fiber [8–10].

Since the fabrication process of a PCF is expensive, it is mandatory to previously simulate the characteristics and performance of the design to be sure it will offer the expected results [11].

The simulation process consists of two clearly differentiated parts: the characterization of the fiber parameters solving the Helmholtz equation and the study with the generalized nonlinear Schrödinger equation (GNLSE) of the propagation of the pulse under the effects of the previously determined parameters [12,13]. In our work, the Helmholtz equation can be treated as an eigenvalue problem [14], and the GNLSE will be solved using spectral techniques.

From a PCF characterization model, a set of curves that relates dispersion parameters with the light wavelength inside the fiber has been obtained [15]. Once these parameters are known, the GNLSE shows the pulse evolution in the fiber both in the time and spectral domains.

There is nothing new in what has been exposed so far; both are well-known problems that have been solved a long time ago. But, while the characterization of the PCF determines the relation between all its parameter and the corresponding wavelength, it is common practice to assume in the propagation a constant working wavelength, usually associated with the center of the pulse [16]. This is an approximation that could be taken in systems where the spectral broadening of the pulse during the simulation is negligible, but the supercontinuum generation is the totally opposite case to that assumption, because our goal is to broaden the spectrum as much as possible [17].

The aim of this work is to study the influence of the wavelength dependence of non-linear and dispersion parameters on the pulse propagation and its effect on the spectrum. Thus, we analyzed if the impact justifies the implementation of this dependency in the usual methods that solve the GNLSE when supercontinuum generation occurs. As it will be shown in the Conclusions, this is the case.

The structure of the paper is as follows. Section 2 will introduce the equations mentioned before, starting with the PCF parameters' characterization through the Helmholtz equation and their application to the proposed structure; secondly, the GNLSE is presented, taking into account the different effects that it includes and its associated terms, as well as the spectral method used to solve it. The supercontinuum generation will also be presented there. Section 3 collects all the results from the simulations and the comparison data between the constant and wavelength-dependent cases. The conclusions will be presented at the end of the whole study.

## 2. Materials and Methods

We have divided this section into four parts; in the first two, we will explain the design of the fiber used and the equations necessary to calculate its most-representative parameters. Subsequently, the wavelength dependence of these parameters will be calculated, and we will end with the application of these results to the GNLSE to see a first generic example of supercontinuum generation.

### 2.1. The PCF Model

The PCFs are characterized by a variety of complex designs built upon a mix of materials that, working as a whole, try to induce interesting behaviors over the light along its propagation, so that, when talking about the PCF design, it would not be misleading to speak about a tailoring process.

In this paper, a very specific design has been chosen to study the supercontinuum phenomena [16]. The next figure shows the transversal section of this fiber. In our case, the core is made of Si and is surrounded by four concentric rings of air holes. The main body of the PCF is made of MgF<sub>2</sub>. Concrete details appear in the comments for Figure 1.

As can be seen, a radial pattern of concentric rings surrounds a central core of silicon. Each of the rings contains  $6n$  air holes, where  $n$  is the order of the ring starting from the inside to the outside. The cladding and core materials are MgF<sub>2</sub> and Si, respectively. Using the Sellmeier equation, with the coefficients presented in Table 1, the dependency of the materials' refractive index can be expressed as a function of wavelength (in  $\mu\text{m}$ ) as [3]:

$$n(\lambda) = \sqrt{1 + A_1\lambda^2(\lambda^2 - B_1)^{-1} + A_2\lambda^2(\lambda^2 - B_2)^{-1} + A_3\lambda^2(\lambda^2 - B_3)^{-1}} \quad (1)$$

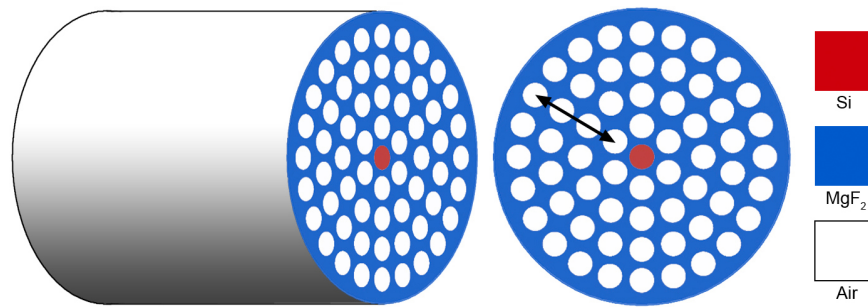


**Figure 1.** Model of the studied PCF. The dimensions in this device are: a core radius of 1.275 μm made of Si, in red in the figure. The air holes have a diameter of 1.2 μm and the lattice constant is  $\Lambda = 2.5 \mu\text{m}$ . The cladding, in blue, is made of MgF<sub>2</sub>. The arrow accounts for three periods of the lattice constant (see Ref. [16]).

The values used for the different coefficients in Equation (1) that appear in Table 1 coming from [18,19] are given below.

**Table 1.** Sellmeier coefficients for MgF<sub>2</sub> and Si.

Material	$A_1$	$A_2$	$A_3$	$B_1 (\mu\text{m}^2)$	$B_2 (\mu\text{m}^2)$	$B_3 (\mu\text{m}^2)$
MgF <sub>2</sub>	0.413	0.505	2.49	0.0013	0.0081	565
Si	10.67	0.003	1.541	0.090	1.288	1,218,816

### 2.2. Helmholtz Equations and Photonic Crystal Fiber Characterization

As explained in the Introduction, the study of the propagation of light through an optical fiber begins with the simulation of its characteristic parameters, which are determined by the internal structure and materials of the fiber. The governing equations of the interaction between this structure and the electric and magnetic fields inside the fiber are the Helmholtz equations [14]:

$$\{\nabla_{\mathbf{t}}^2 + k_0^2\epsilon + \nabla_{\mathbf{t}}[\nabla_{\mathbf{t}}(\ln(\epsilon))]\}\mathbf{e}_{\mathbf{t}} = -\gamma^2\mathbf{e}_{\mathbf{t}} \tag{2}$$

$$[\nabla_{\mathbf{t}}^2 + k_0^2\epsilon + \nabla_{\mathbf{t}}(\ln(\epsilon)) \times \nabla_{\mathbf{t}} \times]\mathbf{h}_{\mathbf{t}} = -\gamma^2\mathbf{h}_{\mathbf{t}} \tag{3}$$

where  $\mathbf{e}_{\mathbf{t}}$  and  $\mathbf{h}_{\mathbf{t}}$  are the transversal components of the electric and magnetic fields for the guided mode,  $\gamma$  the complex propagation constant,  $k_0$  the wavenumber associated with the input pulse, and  $\epsilon$  the dielectric distribution inside the fiber, which depends on its internal structure and constituent materials. By solving one of the equations, Maxwell’s equations allow expressing this solution in terms of the other field distribution.

As can be seen, each of the Helmholtz equations can be expressed as an eigenvalue problem, where the eigenvalues are related to the effective index of the PCF and the eigenvectors coincide with the field distributions for the guided modes.

Starting with the eigenvalue, the effective index can be expressed as:

$$n_{eff} = -\frac{i}{k_0}\gamma = -\frac{i}{k_0}(\alpha + i\beta) = \frac{\beta}{k_0} - i\frac{\alpha}{k_0} \tag{4}$$

where  $\beta$  is the real propagation parameter and  $\alpha$  the loss parameter.

From  $\beta$ , the dispersion orders can be calculated through successive derivation [20]:

$$\beta_n = \frac{\partial^n \beta}{\partial \omega^n} \tag{5}$$

$$\omega = \frac{2\pi c}{\lambda} \tag{6}$$

On the other hand, the integration of the field distributions obtained from the eigenvectors of the system allow calculating the effective area of the modes [20]:

$$A_{eff} = \frac{\left( \int_{-\infty}^{\infty} |F(x, y)|^2 dx dy \right)^2}{\int_{-\infty}^{\infty} |F(x, y)|^4 dx dy} \quad (7)$$

where  $F(x, y)$  refers to the optical field. This parameter represents the light-carrying section of the fiber and is related to the nonlinear parameter, where  $n_2$  is the second-order nonlinear refraction index:

$$\gamma = \frac{n_2 \omega_0}{c A_{eff}} \quad (8)$$

The whole set of parameters presented at this point has a strong dependency on the wavelength, which is introduced in the system through the  $k_0$  value in Equations (2) and (3). In addition, another important factor is the  $\epsilon$  parameter, the dielectric constant, which models the electrical response of the constitutive materials in the PCF.

### 2.3. PCF Parameters' Wavelength Dependency

As we have already pointed out, in our work, we will try to prove the relevance of the dependence on the wavelength of the dispersion parameters used for the propagation of the pulse within the PCF.

In principle, the process to simulate the supercontinuum generation starts by choosing a PCF structure; this part has been explained in a previous section. At this point, we will calculate its parameters with a numerical algorithm for the Helmholtz equations. These parameters will be then employed to numerically solve the generalized NLSE and model the propagation of an input pulse through the given PCF.

A specific numerical method based on centered finite differences [21] was employed to solve the Helmholtz Equations (2) and (3). Once performed, the fiber is characterized over the whole range of the studied wavelengths, obtaining the effective index and effective area relations.

While it is a common practice to assume a working wavelength and refer all the parameters to this value [16], the results that will be presented in the next section show that the parameters' dependency must be calculated individually for each wavelength, for all the wavelengths in the simulation range.

As can be seen in Figure 2, the variability of the dispersion parameters with the wavelength is significant from one end to the another of the simulated range. The impact on the lowest and highest wavelengths is usually neglected with the assumption of constant averaged values. In the Section 3, the influence of each individual value over its associated wavelength in the pulse propagation will be shown.

### 2.4. Generalized Nonlinear Schrödinger Equation and Supercontinuum Generation

The central idea behind supercontinuum generation is to obtain a broad continuous spectrum from a narrower input pulse after its propagation through a nonlinear media, the PCF in this case. Regarding the pulse, its initial delay should be in the femtoseconds regime, which allows the higher-order dispersion effects, among others, to act over it.

The governing equation in this case is the GNLSE, the expression of which is [8]:

$$\frac{\partial E}{\partial z} = \frac{\alpha}{2} E + \sum_{n \geq 2} i^{n+1} \frac{\beta^n}{n!} \frac{\partial^n E}{\partial T^n} + i\gamma \left( E(z, t) \int_{-\infty}^{+\infty} R(T) \times |E(z, T - T')|^2 dT' \right) \quad (9)$$

The three parts of Equation (9) that appear to the left correspond to the following: In the first term,  $\alpha$  accounts for the loss processes; the second part corresponds to the different

partial derivatives that made the group velocity dispersion (GVD) effect; the  $\beta^n$  terms and its dependence on the wavelength is the main part of this work.

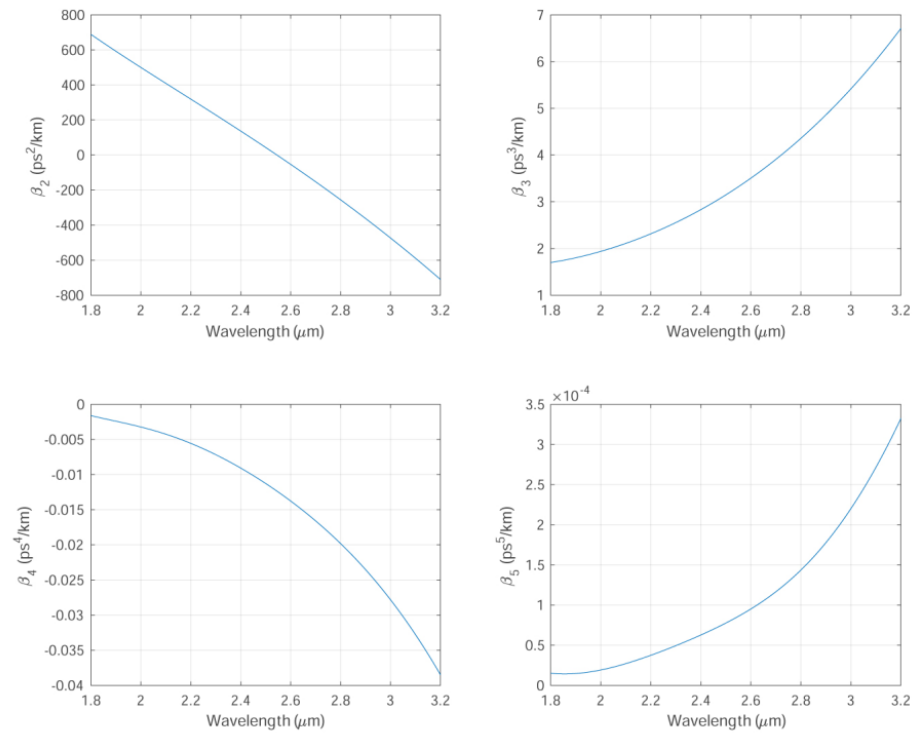


**Figure 2.** Wavelength dependence obtained for linear parameters,  $\beta(\lambda)$ , calculated, which appear in the generalized NLSE. The differences with a constant value approximation in the range of wavelengths studied are noticeable in all of them.

Finally, the nonlinear effects including the Raman effect constitute the third part; here,  $\gamma$  is the nonlinear coefficient, which depends on the mode effective area  $A_{eff}$ , Equation (7), and the nonlinear refractive index. The Raman effects are included through the nonlinear response function  $R(T)$ , which accounts for the instantaneous electronic and delayed Raman contributions, defined as:

$$R(t) = (1 - f_R)\delta(t) + f_R h_R(t) \tag{10}$$

where  $f_R = 0.043$  and  $h_R(t)$  is the Raman response function related to molecular vibrations [22].

In order to resolve the generalized GNLSE, let us separate it into two parts, each one of these accounting for the two different physical effects this equation applies to: the GVD or linear part and the self-phase modulation (SPM) or nonlinear part [20].

After the proposed partitioning, the NLSE has the form:

$$\frac{\partial E(z, t)}{\partial z} = (\hat{L} + \hat{N})E(z, t) \tag{11}$$

Here,  $E$  represents the slowly varying envelope of the solution,  $z$  is the propagation distance, and  $\hat{L}$  and  $\hat{N}$  are the differential operators for the linear (GVD) and the nonlinear (SPM) parts of the equation, respectively.

The separation between both terms is the basis of the time-splitting spectral method used in this work to solve the GNLSE.

We start with the linear operator  $\hat{L}$ :

$$\hat{L} = \sum_{n \geq 2} i^{n+1} \frac{\beta^n}{n!} \frac{\partial^n}{\partial T^n} \tag{12}$$

In a dispersive medium, the GVD term is a result of the differences in the group velocity in a material with respect to the different frequencies that compound the pulse. For a time-splitting spectral approach, this linear part is resolved in the frequency Fourier space.

The nonlinear operator  $\hat{N}$ :

$$\hat{N} = \alpha + i\gamma \left( E(z, t) \int_{-\infty}^{+\infty} R(T) \times |E(z, T - T')|^2 dT' \right) \quad (13)$$

In this case, we use the symmetric propagation scheme:

$$E(\mathbf{x}, t + \Delta t) \approx (e^{-\Delta t \hat{L}/2} e^{-\Delta t \hat{N}} e^{-\Delta t \hat{L}/2}) E(\mathbf{x}, t) \quad (14)$$

Among the multiple numerical algorithms developed to solve the previous equation, the split-step pseudospectral methods are the most-extended due to its accuracy and comparatively lower computational cost [12]. In this paper, the symmetrical split-step Fourier method (S-SSFM) [13] is applied in the simulations.

### 3. Results

In this section, once the object of the study (PCF) and the methods to be used have been stated, we will present the most-relevant results obtained for the generation of supercontinuum when our model is used.

The structure in this part is as follows. We will start by explaining the use of the wavelength dependence of the dispersion propagation parameters, i.e.,  $\beta(\lambda)$ , to solve the problem. Subsequently, the results in both propagation schemes: the constant parameters and the wavelength-dependent scheme, with different pulse widths and peak powers, will be compared, and we will finish by quantitatively defining a parameter to characterize the differences between them.

#### 3.1. Wavelength-Dependent Supercontinuum-Generation Regime

The basis thesis of this paper is that the dependence on the wavelength of the fiber parameters induces a significant impact over the propagation of a solitonic pulse, which must be specially taken into account when simulating processes that cover a wide range of wavelengths like supercontinuum generation. These functional dependences, as appear in Figure 2, have been included in the S-SSFM algorithm.

In Figure 3, we show the results obtained for different propagation stages in the PCF of a input soliton pulse. Starting with the initial values, we can see how relevant the power values appear in the pulse profile throughout the simulations in all the wavelength range [23] In the same figure, we can see how the parameter  $\beta_2$  deviates from a constant value. This constant approach, for the parameters of the generalized NLSE, have been used in previous works [15,16].

Due to these significant discrepancies, we considered it necessary to introduce the dependence on the wavelength for the different-order dispersion parameters and, thus, give a more-adjusted result to the simulated process.

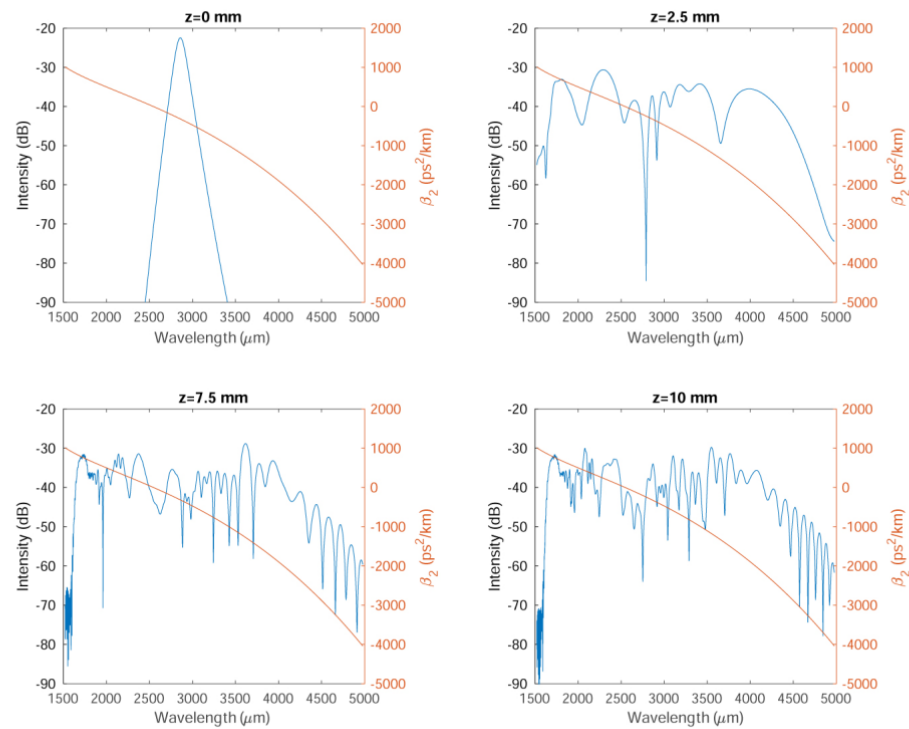


**Figure 3.** Propagation profiles at different distances for the PCF, blue line. The wavelength dependence of the  $\beta_2$  parameter is superimposed. During propagation, the assigned power increases significantly in a wide range of wavelengths compared to the initial profile.

### 3.2. Comparison of Results

Two different input pulses have been simulated for different powers. These simulations have been performed for the constant and functional parameter models, and the results showed the impact of the wavelength dependence over the propagation.

In the first set of simulations, an input soliton pulse of a 50 fs width and a 2860 nm central wavelength were used. Also, the initial peak power values of 250, 500, and 1000 W complete the simulation set. In all cases, the distribution of the spectral intensity is represented on a logarithmic scale.

In addition, Table 2 contains the fiber characteristic parameters, which have been used in the constant model, while the values with the wavelength dependence are those that appear in Figure 2.

**Table 2.** Linear and nonlinear propagation parameters in the wavelength constant case as taken from [16].

$\beta_2$ ( $ps^2/m$ )	$\beta_3$ ( $ps^3/m$ )	$\beta_4$ ( $ps^4/m$ )	$\beta_5$ ( $ps^5/m$ )	$\gamma$ ( $1/W/m$ )
-0.0768	0.0031	$-1.05 \times 10^{-5}$	$7.858 \times 10^{-8}$	5.5

As we can expect, in both simulations, the appearance of notable power values can be observed for wavelengths that are not present in the original pulse. This, as we have already mentioned, is the essence of the supercontinuum-generation phenomenon.

In the approach we propose, i.e., with a dependence on the wavelength of the simulation parameters, we observed a compression of the spectrum obtained with respect to the results of previous studies [16]. This effect is notable even for the lowest of the power values. Figure 4 shows the results for the propagation in the PCF, expressed as the power obtained for each of the wavelengths used.

In Figure 5, we can see the same results obtained in Figure 4, but using the temporal representation. This representation gives us the opportunity to interpret the supercontinuum generation process as being similar to the soliton fission mechanism [24,25].

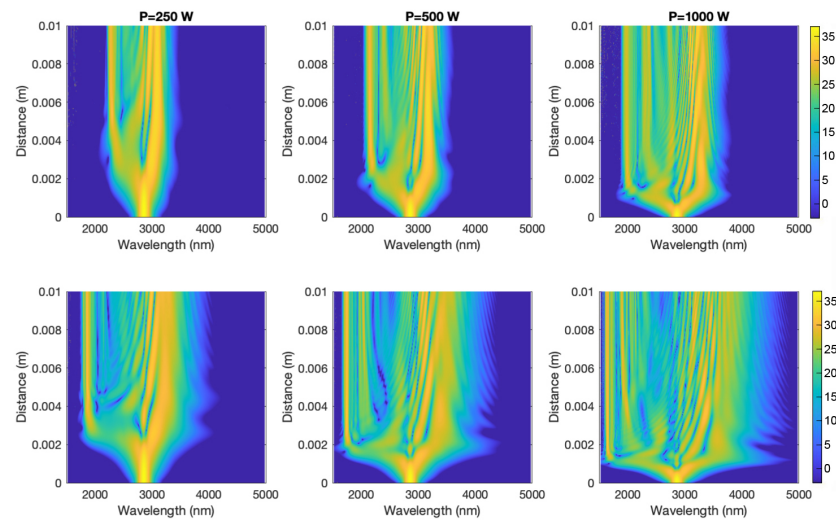


**Figure 4.** The upper row in the figure shows the spectral evolution of a 50 fs pulse when the wavelength dependence is included in the model, while the lower row contains the equivalent cases assuming constant values. The columns represent different input power values. As can be easily seen, the spectral width is narrower over all the propagation distance when the wavelength dependence is taken into account.

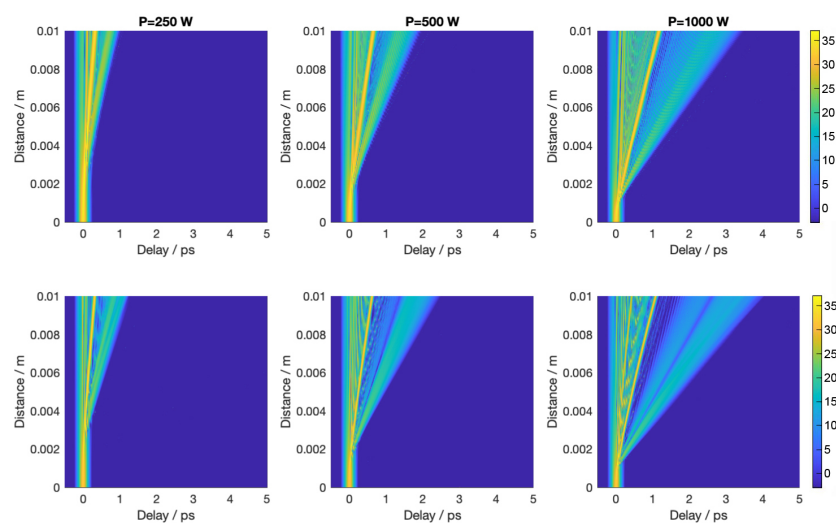


**Figure 5.** In this figure, we can see the evolution, in the time window, of a 50 fs pulse through the PCF. The upper row corresponds to our model with functional dependence, and the lower row corresponds to the case of constant parameters. The columns represent different input power values.

A second case was simulated for a solitonic pulse with the same central wavelength, but with a 500 fs width. The same constant parameters of Table 2 were used, as well as the three same previous input powers. Figures 6 and 7 show the results for the wavelength and time domain representations.

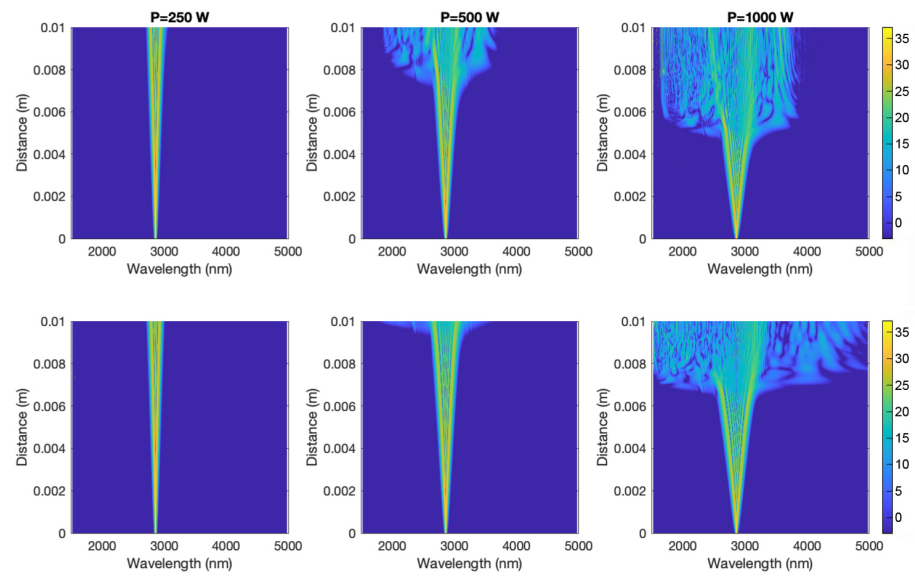


**Figure 6.** Wavelength vs. distance for a 500 fs pulse propagation. The representation criteria are the same as those used in Figure 4.

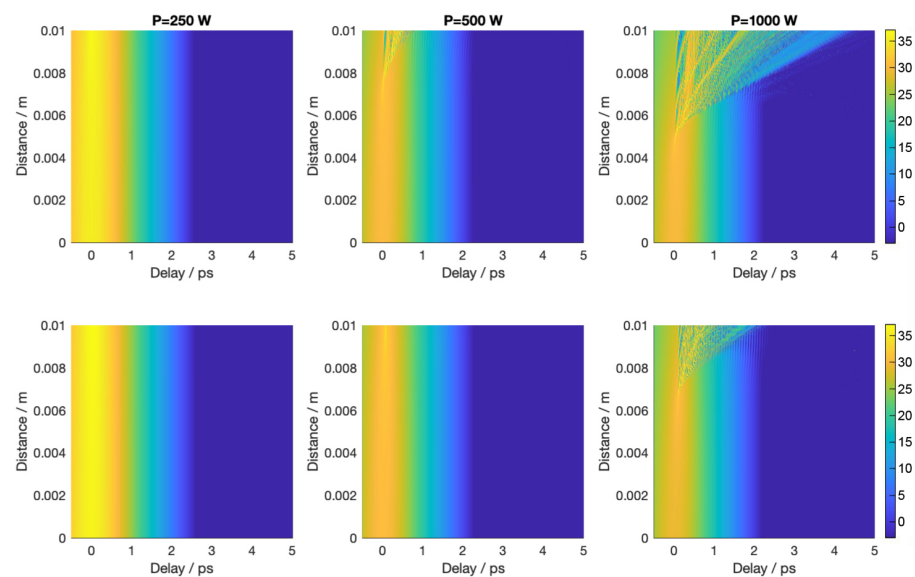


**Figure 7.** Time window vs. distance for a 500 fs pulse propagation. The representation criteria are the same as those used in Figure 5.

### 3.3. Spectral Measuring of the Results

From all the previous results, in our opinion, Figures 4 and 6 are the most-relevant since they show the impact of the wavelength dependence over the spectral width, i.e., the comparison between the top and bottom rows in these figures shows the relevance of our approach to the problem, due to the difference between them.

In order to measure the aforementioned effect, we propose the following scheme:

- Identify the peak power of the spectrum.
- Calculate the desired fraction of power of this peak value (50% in both graphs in the paper).
- Count the total number of wavelengths that exceed this power.
- Determine its percentage over the total of the wavelengths simulated.

This process is repeated over the whole simulation for the constant and dependent models, calculating the difference between both results at each step to obtain Figures 8 and 9.

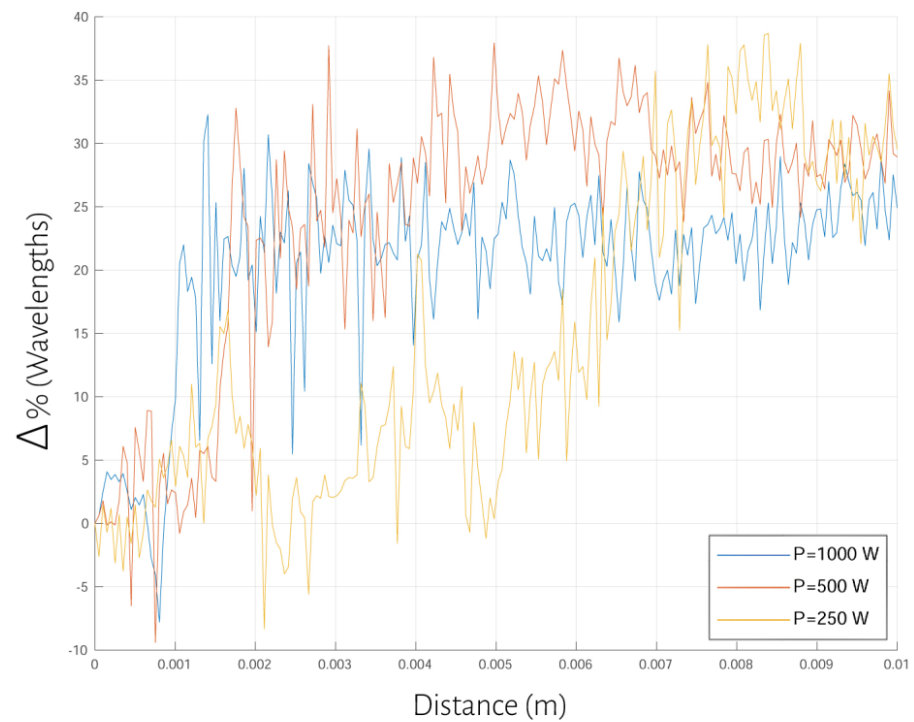


**Figure 8.** Representation of the behavior for the percentage of wavelengths that are above 50% of the maximum peak power value during propagation through the PCF (difference between the constant and dependent cases). This case represents the propagation of the 50 fs pulse. Three different input powers are represented.

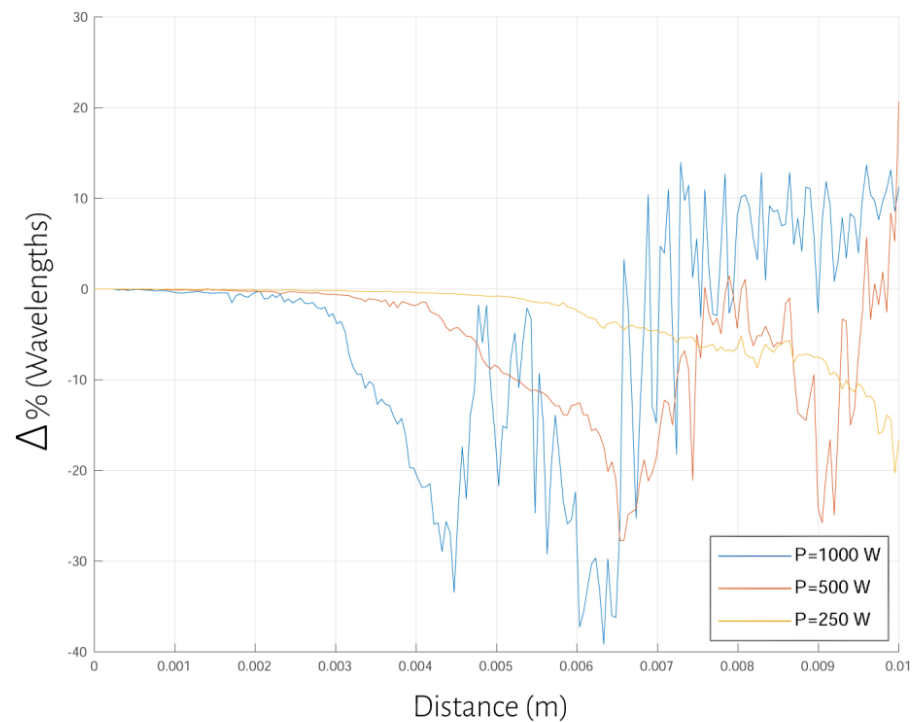


**Figure 9.** Same representation as the previous figure, using, in this case, the 500 fs pulse.

The results showed a difference, which rises up to 30% in the case of the 50 fs pulse, between the number of wavelengths above 50% of the peak power for the constant over the dependent model, being considerably narrower along the whole propagation. This also implies a significative number of wavelengths that are associated with a lower power value than the simplified constant model predicts.

#### 4. Discussion

In this work, we tried to establish, to the best of our knowledge, a different approach to the study of supercontinuum production in the PCF using the wavelength dependence of the dispersion parameters  $\beta(\lambda)$ . As the most-relevant result, we have seen a considerable change in the distribution of the power associated with the different wavelengths.

This effect, in our opinion, is not negligible, as can be seen in the case of the narrow pulses in Figure 8 or in the case of the wider pulses for higher powers in Figure 9. In such a wavelength-dependent effect, as the supercontinuum generation is, we considered that this result must be taken into account in order to design better and more-accurate experimental devices.

To finish this section, some future lines of research associated with the proposed results could be proposed, e.g., from a theoretical point of view, the study could be extended to different geometries of the device or include the wavelength dependency for the rest of the parameters that appear in the generalized NLSE or, in a more-applied way, the study of the sensitivity characteristics when the PCFs are used as detectors. In this last direction, our group has already begun with some simulations.

**Author Contributions:** P.R. and D.M.-M. designed the simulations; A.O.-M. and A.D.-S. developed the theoretical part. All authors contributed to the analysis and writing of the results of the work. All authors have read and agreed to the published version of the manuscript.

**Funding:** This research received no external funding. We would like to thank the SICOMFITIC176 group of the Physics Department of the University of Córdoba for their support during the research process.

**Institutional Review Board Statement:** Not applicable.

**Informed Consent Statement:** Not applicable.

**Data Availability Statement:** We are considering the possibility of creating a git-hub-type repository with the developed material. The raw data supporting the conclusions of this article will be made available by the authors on request.

**Acknowledgments:** The authors appreciate the support of C. Quesada Padilla with the grammatical corrections of the final document.

**Conflicts of Interest:** The authors declare no conflicts of interest.

#### Abbreviations

The following abbreviations are used in this manuscript:

PCF	photonic crystal fiber
GNLSE	generalized nonlinear Schrodinger equation
SPM	self-phase modulation
GVD	group velocity dispersion
S-SSFM	symmetrical split-step Fourier method

#### References

1. Joannopoulos, J.D.; Villeneuve, P.R.; Fan, S. Photonic Crystals. *Solid State Commun.* **1997**, *102*, 165–173. [[CrossRef](#)]
2. She, Y.; Liu, D.; Li, J.; Yao, M.; Zheng, Y.; Wu, F. Tunable wide-angle high-efficiency polarization selectivity based on a one-dimensional photonic crystal containing elliptical metamaterials. *Phys. Lett. A* **2024**, *494*, 129299. [[CrossRef](#)]
3. Knight, J.C. Photonic Crystal Fibres. *Nature* **2003**, *424*, 847–851. [[CrossRef](#)] [[PubMed](#)]
4. Russell, P.S.J. Photonic-crystal fibers. *J. Light. Technol.* **2006**, *24*, 4729–4749. [[CrossRef](#)]

5. Pinto, A.M.R.; López-Amo, M. Photonic Crystal Fibers for Sensing Applications. *J. Sens.* **2012**, *2012*, 598178. [[CrossRef](#)]
6. Luan, F.; Knight, J.; Russell, P.; Campbell, S.; Xiao, D.; Reid, D.; Mangan, B.; Williams, D.; Roberts, P. Femtosecond soliton pulse delivery at 800 nm wavelength in hollow-core photonic bandgap fibers. *Opt. Express* **2004**, *12*, 835–840. [[CrossRef](#)] [[PubMed](#)]
7. Cheo, P.L.; Liu, A.; King, G.G. A high-brightness laser beam from a phase-locked multicore Yb-doped fiber laser array. *IEEE Photon. Technol. Lett.* **2001**, *13*, 439–441. [[CrossRef](#)] [[PubMed](#)]
8. Dudley, J.M.; Taylor, J.R. (Eds.) *Supercontinuum Generation in Optical Fibers*; Cambridge University Press: Cambridge, UK, 2010.
9. Wadsworth, W.J.; Ortigosa-Blanch, A.; Knight, J.C.; Birks, T.A.; Martin, T.P.; Russell, P.S.J. Supercontinuum generation in photonic crystal fibers and optical fiber tapers: A novel light source. *J. Opt. Soc. Am. B* **2002**, *19*, 2148–2155. [[CrossRef](#)]
10. Baselt, T.; Nelsen, B.; Lasagni, A.F.; Hartmann, P. Supercontinuum Generation in the Cladding Modes of an Endlessly Single-Mode Fiber. *Appl. Sci.* **2019**, *9*, 4428. [[CrossRef](#)]
11. Joannopoulos, J.D.; Johnson, S.G.; Winn, J.N.; Meade, R.D. *Photonic Crystals: Molding the Flow of Light*, 2nd ed.; Princeton University Press: Princeton, NJ, USA, 2008.
12. Taha, T.R.; Ablowitz, M.I. Analytical and numerical aspects of certain nonlinear equations: II Nonlinear Schrodinger Equation. *J. Comput. Phys.* **1984**, *55*, 203–230. [[CrossRef](#)]
13. Yoshida, H. Construction of higher order symplectic integrators. *Phys. Lett. A* **1990**, *150*, 262–268. [[CrossRef](#)]
14. Saleh, B.E.A.; Teich, M.C. *Fundamentals of Photonics*; Wiley Series in Pure and Applied Optics; John Wiley & Sons: New York, NY, USA, 2019.
15. Huttunen, A.; Törmä, P. Effect of wavelength dependence of nonlinearity, gain, and dispersion in photonic crystal fiber amplifiers. *Opt. Express* **2005**, *13*, 4286–4295. [[CrossRef](#)]
16. Dashtban, Z.; Salehi, M.R.; Abiri, E. Supercontinuum generation in near- and mid-infrared spectral region using highly nonlinear silicon-core photonic crystal fiber for sensing applications. *Photonics Nanostruct. Fundam. Appl.* **2021**, *46*, 100942. [[CrossRef](#)]
17. Jones, W.J.; Stoicheff, B.P. Inverse Raman Spectra: Induced Absorption at Optical Frequencies. *Phys. Rev. Lett.* **1964**, *13*, 657–659. [[CrossRef](#)]
18. Dodge, M.J. Refractive Properties of Magnesium Fluoride. *Appl. Opt.* **1984**, *23*, 1980–1985. [[CrossRef](#)] [[PubMed](#)]
19. Salzberg, C.D.; Villa, J.J. Infrared Refractive Indexes of Silicon, Germanium and Modified Selenium Glass. *J. Opt. Soc. Am.* **1957**, *47*, 244–246. [[CrossRef](#)]
20. Agrawal, G.P. *Nonlinear Fiber Optics*, 6th ed.; Academic Press: San Diego, CA, USA, 2019.
21. Díaz-Soriano, A.; Ortiz-Mora, A.; Dengra, A. Comparative study of numerical methods used in modeling photonic crystal fibers. *Microw. Opt. Technol. Lett.* **2013**, *55*, 1049–1053. [[CrossRef](#)]
22. Lin, Q.; Agrawal, G.P. Raman response function for silica fibers. *Opt. Lett.* **2006**, *31*, 3086–3088. [[CrossRef](#)]
23. Arteaga-Sierra, F.R.; Antikainen, A.; Agrawal, G.P. Soliton dynamics in photonic-crystal fibers with frequency-dependent Kerr nonlinearity. *Phys. Rev.* **2018**, *98*, 013830. [[CrossRef](#)]
24. Tai, K.; Hasegawa, A.; Bekki, N. Fission of optical solitons induced by stimulated Raman effect. *Opt. Lett.* **1988**, *13*, 392–394. [[CrossRef](#)] [[PubMed](#)]
25. Sharafali, A.; Nithyanandan, K. A theoretical study on the supercontinuum generation in a novel suspended liquid core photonic crystal fiber. *Appl. Phys. B* **2020**, *126*, 55. [[CrossRef](#)]

**Disclaimer/Publisher’s Note:** The statements, opinions and data contained in all publications are solely those of the individual author(s) and contributor(s) and not of MDPI and/or the editor(s). MDPI and/or the editor(s) disclaim responsibility for any injury to people or property resulting from any ideas, methods, instructions or products referred to in the content.